

---

This is an electronic reprint of the original article.

This reprint may differ from the original in pagination and typographic detail.

Ornaghi, Heitor L.; Almeida, José Humberto S.; Monticeli, Francisco M.; Neves, Roberta M.; Cioffi, Maria Odila H.

**Time-temperature behavior of carbon/epoxy laminates under creep loading**

*Published in:*

Mechanics of Time Dependent Materials

*DOI:*

[10.1007/s11043-020-09463-z](https://doi.org/10.1007/s11043-020-09463-z)

Published: 07/09/2020

*Document Version*

Publisher's PDF, also known as Version of record

*Published under the following license:*

CC BY

*Please cite the original version:*

Ornaghi, H. L., Almeida, J. H. S., Monticeli, F. M., Neves, R. M., & Cioffi, M. O. H. (2020). Time-temperature behavior of carbon/epoxy laminates under creep loading. *Mechanics of Time Dependent Materials*. <https://doi.org/10.1007/s11043-020-09463-z>



# Time-temperature behavior of carbon/epoxy laminates under creep loading

Heitor L. Ornaghi Jr.<sup>1</sup> · José Humberto S. Almeida Jr.<sup>2</sup>  · Francisco M. Monticeli<sup>1</sup> · Roberta M. Neves<sup>3</sup> · Maria Odila H. Cioffi<sup>1</sup>

Received: 6 February 2020 / Accepted: 8 August 2020  
© The Author(s) 2020

**Abstract** The time-temperature creep behavior of advanced composite laminates is herein determined through a comprehensive set of experiments and analytical modeling. A complete structure *versus* property relationship is determined through a wide range of temperature and applied stress levels at the three states of the composite: glassy, glass transition, and rubbery regions. Weibull, Eyring, Burger, and Findley models are employed to predict the experimental data and to better elucidate the material behavior. Experimental creep tests are carried out under ten min and two days aiming at calibrating fitting parameters, which are essential to validate short-term creep tests. The Weibull and Eyring models are more suitable for determining the time-temperature superposition (TTS) creep response in comparison to the Burger and Findley models.

**Keywords** Advanced composites · Viscoelasticity · Creep · Time-temperature superposition

## 1 Introduction

Creep in carbon fiber reinforced polymer (CFRP) composite materials may lead to unexpected stress redistribution over time, which can influence the durability and life service of composite structures (Gao et al. 2018; Mohammad et al. 2018; Wang et al. 2019). Significant progress has been carried out in terms of the time-independent behavior of CFRP composites. However, in engineering applications, compliance and deformation properties are stress- and time-dependent (Almeida et al. 2018a, 2018b; Ornaghi et al. 2020).

---

✉ J.H.S. Almeida Jr.  
[humberto.almeida@aalto.fi](mailto:humberto.almeida@aalto.fi); [jhsajunior@globomail.com](mailto:jhsajunior@globomail.com)

<sup>1</sup> Department of Materials and Technology, Sao Paulo State University, 12516-410 Guaratinguetá, SP, Brazil

<sup>2</sup> Department of Mechanical Engineering, Aalto University, 02150 Espoo, Finland

<sup>3</sup> PPGE3M, Federal University of Rio Grande do Sul, Av. Bento Gonçalves 9500, Porto Alegre, RS, Brazil

The long-term of such high-performance composites is important to be quantified, given the viscoelastic nature of polymeric matrices (Guedes 2006). A very few studies are found in the literature dealing with the long-term mechanical behavior relating thermoset matrix composites (Sullivan 1990; Sullivan et al. 1993; Hu and Sun 2000; Fancey 2001, 2005; Alrahlah et al. 2018). Fancey (2001, 2005) mentioned the importance of low-stress creep response for the tensile modulus prediction. A low-stress level analysis allows a fast and inexpensive way in relation to structure *versus* property relationship (Alrahlah et al. 2018; Fancey 2001, 2005). General failure mechanisms are present in two main scales, (i) microscopic and (ii) macroscale mechanisms that arise from microstructural changes (Khan et al. 2015). According to Alderliesten (2015), a merely phenomenological analysis could neglect important physical aspects at the microscale. In other words, the microstructural mechanical performance is an important factor for determining macrostructural changes, considering physical aspects (Alderliesten 2015; Khan et al. 2015). In this perspective, dynamic-mechanical analysis (DMA) allows determining the creep behavior and observe microstructural changes (molecular mobility) (Alrahlah et al. 2018; Fancey 2001; Mano et al. 2004). For instance, the elastic modulus can be predicted by measuring different load levels and considering the reciprocal of the gradient from a linear regression line, showing good correlation with the experimental data analyzed, encouraging to note that the instantaneous deformation values agree with available tensile modulus data (Fancey 2001).

The performance of composites structures will be understood by combining experimental with computational approaches (Sullivan 1990; Sullivan et al. 1993; Hu and Sun 2000). Sullivan et al. (1993) demonstrated that short-term (momentary) creep of a composite is a fundamental viscoelastic response to an applied load at constant time. On the other hand, long-term creep is not a fundamental material response. The main reason is that short-term tests do not allow significant loss of structural integrity to occur while the system is responding to an applied load. Therefore it is necessary to extrapolate the obtained information from relatively short-term creep tests to long-term cases. Studies related to creep response have been performed by Gates et al. (1997) and Struik (1977), but there is still a lack in the literature about microstructure *versus* properties relationship related to creep and recovery behaviors for polymeric systems. Creep and recovery can be represented by analogous mechanical models based on the Weibull distribution function and Eyring model (Fancey 2001, 2005), where a more complete understanding of the microstructure is elucidated along with other analytical models.

This paper aims at characterizing the creep behavior of carbon/epoxy composites using three different load levels at several temperature ranges. In addition, recovery tests are carried out in glassy, glass transition region, and elastomeric state using the same loads. The time-temperature superposition (TTS) principle is performed at three load levels for the creep tests.

## 2 Manufacturing

A biaxial  $+45^\circ/-45^\circ$  carbon fiber non-crimp fabric was used (Hexcel IM7 12K GP). The fabrics were cut in different directions to achieve the desired stacking sequence. The areal density of the NCF was  $410 \text{ g}\cdot\text{m}^{-2}$ , and specific density was  $1.78 \text{ g}\cdot\text{cm}^{-3}$ . The epoxy resin used was an RTM-6 from Hexcel. The layers were stacked in a way to avoid bending of the fabric during the resin flow. The final stacking sequence was a balanced and symmetric quasi-isotropic laminate  $[0/90/45/-45]_{2S}$ . The composites were processed by vacuum-assisted resin transfer molding (VARTM) using a Radius 2100cc RTM Injector with 0.25

MPa of injection pressure, 120 °C of injection temperature (viscosity of 90 mPa·s), 0.05 MPa of vacuum, and curing at 180 °C for 120 min (Monticeli et al. 2020).

### 3 Viscoelastic models

The creep behavior of the composites was characterized by Findley and Burger models. Weibull-based and Eyring models were also implemented, aiming to represent the distribution of viscoelasticity elemental failures and the energies involved in the process. Creep tests were performed at three selected temperatures in the three main regions of the material (glassy, glass transition, and elastomeric states). Finally, 2-day creep tests were performed. The TTS analysis was performed using different isothermal temperatures from increments of 20 °C from glassy to elastomeric region (temperature range from 30 to 210 °C).

#### 3.1 Viscoelastic modeling for the composites

The long-term behavior of the composites for TTS individual curves (10-min test in each isotherm) and for 2-day creep tests was modeled by Findley (Eq. (1)) and Burger (Eq. (2)) laws, which allows a good approximation of primary and secondary creep phenomena, as follows:

$$\varepsilon(t) = \varepsilon_0 + At^n, \quad (1)$$

$$\varepsilon_B = \frac{\sigma_0}{E_M} + \frac{\sigma_0}{E_K} \left(1 - e^{-\frac{t}{\tau}}\right) + \frac{\sigma_0}{n_M} t, \quad (2)$$

where  $\varepsilon_0$  is the instantaneous deformation,  $A$  and  $n$  are constants,  $E_M$  and  $n_M$  are the modulus and viscosity of Maxwell, respectively,  $E_K$  and  $n_K$  are the modulus and viscosity of Kelvin, respectively,  $\tau = n_K/E_K$  is the retardation time to produce 63.2% or  $(1 - e^{-1})$  of the total deformation of the Kelvin unity, and  $\sigma_0$  is the initial applied stress.

Creep curves were also fitted following the Weibull distribution function. For creep under an applied load, the total strain is given by

$$\varepsilon_{tot}(t) = \varepsilon_i + \varepsilon_c \left[1 - \exp\left(-\left(\frac{t}{\eta_c}\right)^{\beta_c}\right)\right], \quad (3)$$

where  $\varepsilon_i$  is the initial instantaneous strain from the load application, and the function  $\varepsilon_c$  represents creep strain, which is determined by the characteristic life ( $\eta_c$ ) and shape ( $\beta_c$ ) parameters as functions of load duration  $t$ . When the load is removed, there may be some instantaneous (elastic) strain recovery, which is then followed by time-dependent recovery strain. For that, the Eyring-based model was used:

$$\sigma_{rel}(t) = A \tanh\left[\tanh(B) \exp\left(-\frac{t}{\tau}\right)\right] + \sigma_e, \quad (4)$$

in which  $A$  and  $B$  are constants,  $\tau$  is the relaxation time, the parameter  $\sigma_e$  is the final stress as  $t$  tends to infinity.

Experimentally, long-term creep behavior is often impractical because of the extremely long time required. Thus predicting the long-term creep behavior using a short-term testing has gained considerable attention. One of the most common extrapolation techniques is

the TTS. The mathematical procedure consists in shifting the curves from tests at different temperatures horizontally along a logarithmic time axis to generate a single curve known as the master curve. Thus a long-term experiment can be replaced by shorter tests at higher temperatures. The shifting distance is called the shift factor. The shift factors of a thermorheologically simple material (in which TTS holds) can be related to temperature using either the Williams–Landel–Ferry (WLF) or Arrhenius equations. The WLF equation is defined as

$$\log a_T = \frac{-C_1(T - T_0)}{C_2 + (T - T_0)}, \quad (5)$$

where  $a_T$  is the horizontal (or time) shift factor,  $C_1$  and  $C_2$  are constants,  $T_0$  is the reference temperature (K), and  $T$  is the test temperature (K).

### 3.2 Testing

Aiming to trace specific artificial defects of the processed composites, C-Scan was performed. Acoustic Inspection C-Scan Microscopy was performed using a MI-SCAN equipment with an insert program MUIS32 from MATEC for data achievement. Data was collected using a concave transducer of 2.25 MHz frequency and analyzed using I-view software, also developed by MATEC with color associated images.

Void and fiber volume fractions were determined according to ASTM D3171-15 standard. Three specimens of dimensions  $10 \times 50 \times 3 \text{ mm}^3$  were initially tested and after immersed in heated nitric acid ( $60^\circ\text{C}$  during 1.5 h) for complete epoxy burn off. The remained fibers were washed, dried, and posteriorly weighted, and then both fiber volume and void fractions could be measured.

Creep experiments have been performed using a DMA Q800 equipment using the three-point bending clamp. Firstly, 2-day creep test was performed at  $50^\circ\text{C}$  and 5 MPa to evaluate creep behavior and compare to short-time experiments. A 10-min soak time was applied to ensure that the specimen reached the equilibrium after each test temperature for all procedures. Then the controlled stress was applied and kept constant for 10 min for subsequent analysis itself. The selected stresses are much below than the yield stress of the composites under investigation. Therefore the emergence of viscoplastic strain has been negligible (in the case of 2-day and creep tests). For creep TTS analysis, ten different temperatures (from  $30^\circ\text{C}$  to  $210^\circ\text{C}$  in steps of  $20^\circ\text{C}$ ) at three stress levels (1, 2.5, and 5 MPa) were carried out involving all three main regions of the composites. The curve fittings have been carried out using Datafit Software.

## 4 Results and discussion

To verify the resin impregnation across the laminate, C-Scan test is presented in Fig. 1. The scale represents the attenuation signal: white color means 100% return of the signal, and black color represents 0% of the emitted signal. The composite has excellent resin impregnation in all regions (30%–40% of attenuation). The density of the composite is  $1.52 \pm 0.01 \text{ g.cm}^{-3}$ , fiber volume fraction is 59.6%, and void content is 3.44% (Lorandi et al. 2018).

In Fig. 2(a), creep behavior performed for two days is fitted with 10 min at  $50^\circ\text{C}$  for comparison. A 2-day creep follows a similar plateau trend to 10-min test validating the small time chosen for further analysis. Figure 2(b–d) shows the creep behavior of the composites at three load levels and all temperatures in the range tested (from 30 to  $210^\circ\text{C}$ ).

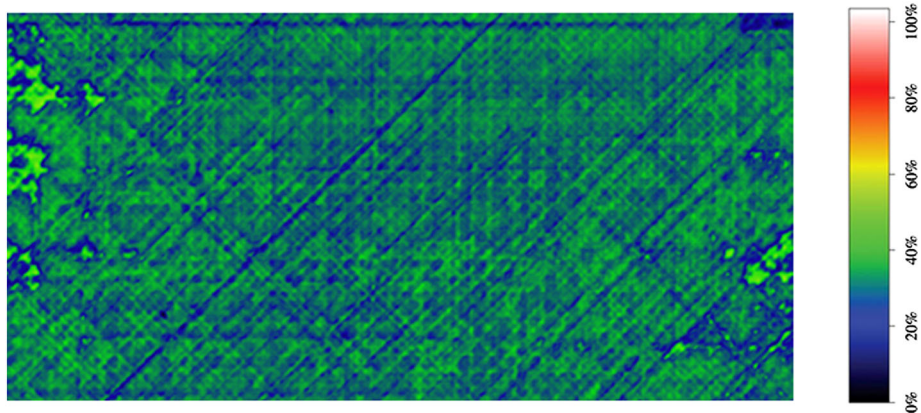


**Fig. 1** C-Scan results for the laminate composite studied (Color figure online)

At low stress levels and temperatures, low instantaneous deformation is observed, once there are not many amounts of polymer segments to be activated to involve the creep response in short time. With increasing time, more segments are activated and bring in relatively velocity of orientation of polymer segments and entanglements, and thus higher creep rate occurs (Fig. 2e). The large instantaneous deformation at higher stresses is an indicative that many segments are oriented to some extent along the stress direction in a short time, and thereafter orientational hardening makes it difficult to get further reorientation and rearrangement of polymer chains and entanglements due to relatively small stress level (Fancey 2005; Yang et al. 2006a, 2006b; Xu et al. 2010).

The temperature follows the same trend as the stress. The relaxation process in laminated composites is a reflection of the difficulty/easiness of the matrix in rearranging polymer segments between crosslinks due to some internal/external imposed stress (Lomellini 1992; Ornaghi et al. 2015). Below the  $T_g$  (blue curves in Fig. 2(e)), the deformation imposed in the chain segments is primarily elastic (polymeric chains are in a frozen-in state) and the molecular slippage resulted in the viscous flow is low. In the rubbery region (red curves in Fig. 2(e)) the molecular segments are relatively free to move, and hence the damping is low. At the  $T_g$  (black curves in Fig. 2(e)) the molecular chains begin to move, and every time a frozen-in segment begins to move, its excess of energy is dissipated as heat (Lomellini 1992; Lorandi et al. 2016; Matsuoka 1993). Frozen-in segments can restore more energy for a given energy and deformation than rubbery segments. The maximum damping leads to the most of the chain segments taking part in a cooperative motion reflecting in a more accentuated transition from elastic to viscous regions in the creep test, as can be seen in Fig. 3 (Fancey 2005; Lorandi et al. 2018). According to Fig. 3 (representative curve at 2.5 MPa), the strain tends to increase as temperature approximates  $T_g$ , decreasing thereafter and behaving similarly at both glassy and elastomeric regions. For all load levels, a similar behavior, nonetheless, is observed.

To apply the TTS procedure, the results presented in Figs. 2(a–c) are replotted in a log-log scale, as shown in Figs. 4(a–c). At lower temperatures, more energy is needed to mobilize the molecular chains during creep; consequently, the deformation over time is lower. At higher stress, more segments are strained in a short time, leading to higher deformation at the same time interval. The smooth master curves (TTS) over long time periods are obtained using a reference temperature of 30 °C (Fig. 4d). The master curves show that creep resistance

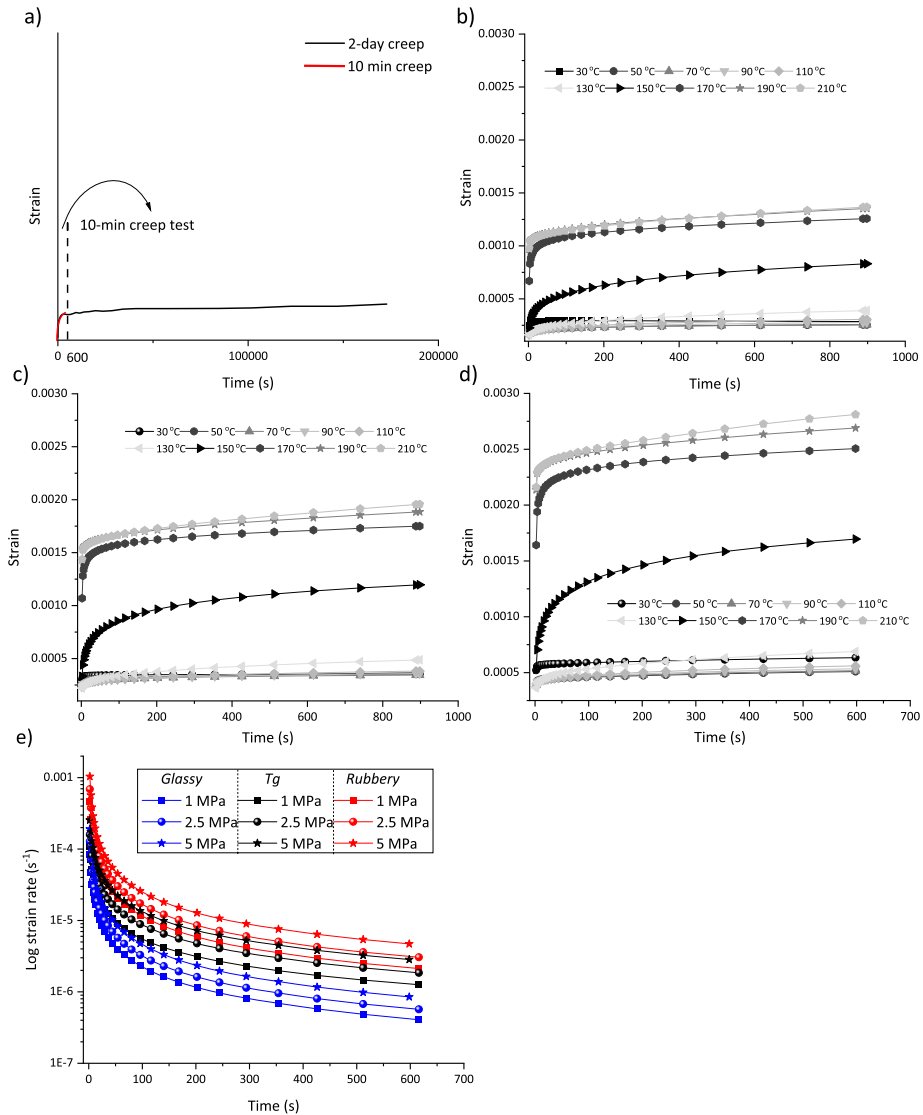


**Fig. 2** Creep behavior of the composite studied: **a)** comparative 2-day and 10-min tests at 150 °C under 5 MPa; creep response of the composites under several temperatures for stress levels of **b)** 1 MPa, **c)** 2.5 MPa, **d)** 5 MPa; and **e)** strain rate against time for the three stress levels applied at the glassy, glass transition, and rubbery states (Color figure online)

decreases with increasing the applied load. Higher load levels result in higher deformations, mainly from the glass transition temperature to rubbery state. According to Yang et al. (2006b), creep response in function of time can be divided into three different stages: I, primary (glassy); II, secondary (viscoelasticity); and III, tertiary (rubbery). The instantaneous elongation is due to the elastic or plastic deformation of polymer once the external load is applied, and this stage is time-independent. The TTS curves allow predicting the behavior in a range from  $10^{-6}$  to  $10^3$  s (c.a. three centuries). In the primary creep stage, the creep rate

**Fig. 3** Creep strain (%) for the composite tested at 2.5 MPa in all temperatures

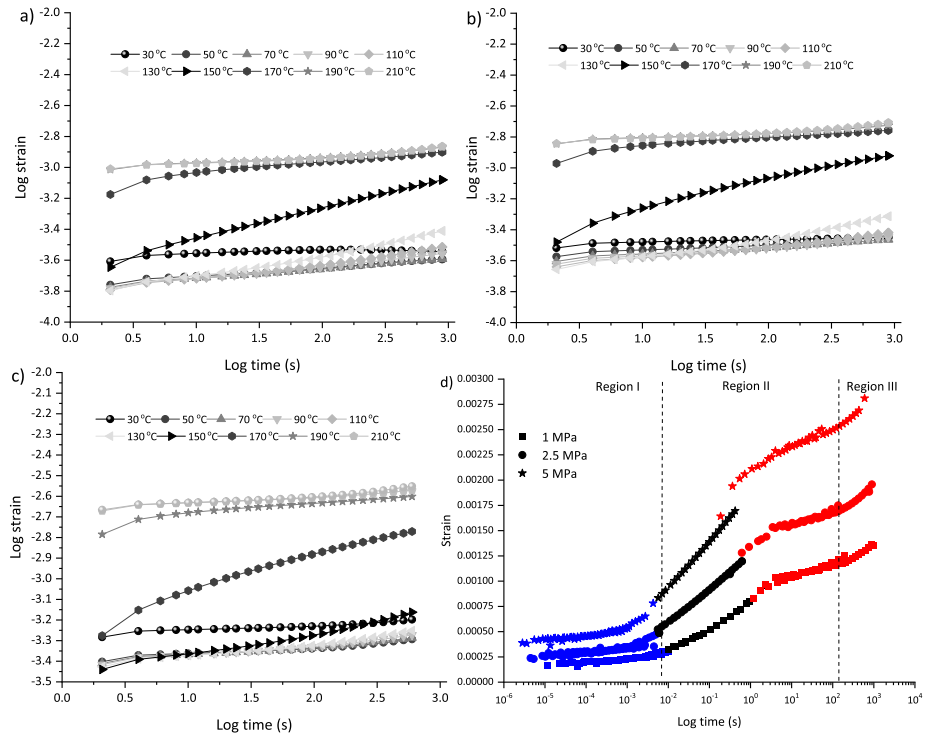
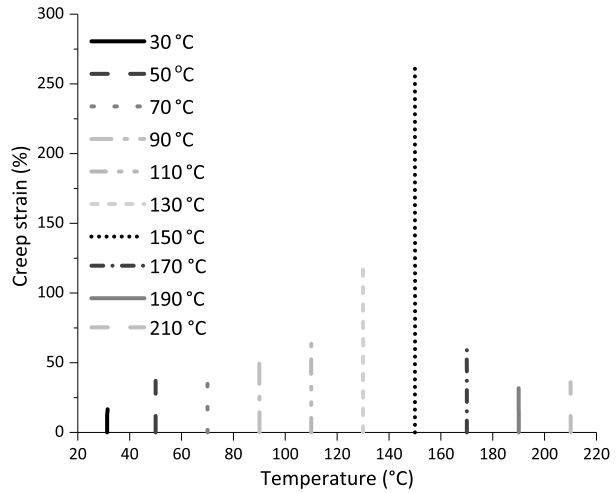


**Fig. 4** Log strain vs log time at a) 1 MPa, b) 2 MPa, c) 5 MPa, and d) TTS curves for all stress levels (Color figure online)

starts at relatively high value, then decreases rapidly with time, which may be resulted from the slippage and orientation of polymer chains under constant stress. After a certain period, the creep rate reaches a steady state at the secondary creep stage, in which the viscoelastic



flow in the polymer occurs and the duration is relatively long when under low stress. Then the material falls into the tertiary creep stage, where the creep rate rapidly increases, and final creep rupture or advanced necking occurs. These results suggest that a beginning of rupture can be observed for all load levels according to classic creep curves (Findley and Davis 2013; Yang et al. 2006a). Hence TTS curves are successfully applied using short-term experiments.

Findley and Burgers models were employed to fit the experimental data (Fig. 5). The fitted parameters for three different temperatures in glassy (50 °C), glass transition (150 °C), and rubbery (210 °C) regions are summarized in Table 1. Independently of the applied load, the best fit is found for the samples at the  $T_g$  for all models (Figs. 5(a–c)). Figure 5(d) shows fitting for all models using the TTS curves. The TTS curves allow estimating the behavior of materials not tangible experimentally. We noticed that at the  $T_g$ , there is an abrupt creep deformation independently of the stress level applied. This phenomenon is more pronounced for higher stress levels. In addition, both Weibull and Eyring models fit the experimental data very well, whereas the Burger and Findley models have poorer fitting.

Findley's parameters ( $A$  and  $n$ ) are constants relatively similar at glassy and elastomeric regions, whereas the same parameters are higher at the  $T_g$ , being more temperature-dependent than stress-dependence. The instantaneous deformation tends to increase with higher temperatures and loads.

In relation to Burger's parameters, the time-independent elasticity  $E_M$  represents the Maxwell spring in the instantaneous creep strain, which is recoverable after removing the applied load. This parameter is temperature-dependent because the bulk material tends to become softer with temperature, which decreases the instantaneous modulus (Fancey 2005; Xu et al. 2010; Yang et al. 2006a, 2006b). This parameter can be associated with the storage modulus in the glassy region, where higher temperatures decrease the modulus when compared to the same static stress applied (Almeida et al. 2018a, 2018b). These results suggest that it is difficult to have some viscous flow on the bulk material due to a higher elastic deformation at a short-time response. Therefore more chain molecular cooperativity is necessary for higher stresses, in which an enhanced mobility of amorphous chain is harder to achieve, increasing the time-independent elasticity values by the applied stress applied (Fancey 2001).

The retardancy elasticity  $E_k$  and viscosity  $\eta_k$  are associated with the stiffness and viscous or orientated flow of amorphous polymer chains in short term (Fancey 2005; Yang et al. 2006a, 2006b; Xu et al. 2010; Lorandi et al. 2016). Both parameters show similar dependency on temperature and stress. When temperature increases and tends to achieve the glass transition phase, amorphous polymers become more active and promptly oriented in a short period. The viscous slippage of the molecules becomes easier to achieve upon temperature. Hence both parameters decrease by increasing the temperature due to a greater energy absorption by the active polymer chains. In addition, the long-chained molecules are not able to withstand deformation at higher temperatures as they become increasingly active due to higher energy absorption. Polymer chains thereafter have a high potential energy site due to orientational hardening, which increases the values according to the applied stress (Lomellini 1992; Matsuoka 1993; Fancey 2005; Yang et al. 2006a, 2006b; Xu et al. 2010; Lorandi et al. 2016). The retardation time  $\tau$  decreases with increasing the applied stress when compared to the same temperature due to higher molecular mobility. However, when comparing different stresses, the values obtained at glassy and rubbery regions are more similar in comparison to that obtained at the  $T_g$ . At the glassy region the elastic response is predominant, whereas in the rubbery region the viscous response prevails. At the  $T_g$ , there is a greater release of energy, which is eliminated as heat in the frozen-in chains, achieving their maximum at the  $T_g$ .

**Table 1** Findley and Burger parameters obtained at 50 °C, 150 °C, and 210 °C

Model tested at 50 °C	Parameters	1 MPa	2.5 MPa	5 MPa
Findley's power law	A	2.57E-15	1.16E-15	1.19E-16
	n	0.2660	0.3171	0.2746
	$\varepsilon_0$	1.55E-4	2.29E-4	3.06E-4
	SS*	2.88E-8	6.23E-8	1.22E-7
	R <sup>2</sup>	0.526	0.459	0.440
Burgers	E <sub>M</sub> (MPa)	1.22E+6	2.04E+23	2.05E+23
	E <sub>K</sub> (MPa)	4785.93	8248.53	11367.02
	$\eta_K$ (MPa.s)	6283.63	8491.85	10508.25
	$\eta_M$ (MPa.s)	1.57E+7	3.15E+7	3.74E+7
	$\sigma\tau$ (s)	1.31	1.03	0.92
	SS*	2.16E-9	1.29E-9	8.29E-10
	R <sup>2</sup>	0.964	0.989	0.996
Model tested at 150 °C	Parameters	1 MPa	2.5 MPa	5 MPa
Findley's power law	A	4.70E-12	1.79E-12	4.53E-12
	n	0.3787	0.3420	0.3330
	$\varepsilon_0$	2.18E-4	3.28E-4	4.71E-4
	SS*	7.67E-8	2.10E-7	4.08E-7
	R <sup>2</sup>	0.932	0.910	0.896
Burgers	E <sub>M</sub> (MPa)	7935.53	2.09E+26	1.05E+26
	E <sub>K</sub> (MPa)	2595.70	3226.11	4422.03
	$\eta_K$ (MPa.s)	3.58E+4	2.41E+4	25021.69
	$\eta_M$ (MPa.s)	2.46E+6	4.45E+6	4.29E+6
	$\tau$ (s)	13.83	7.49	5.66
	SS*	5.33E-8	1.39E-7	1.92E-7
	R <sup>2</sup>	0.953	0.941	0.951
Model tested at 210 °C	Parameters	1 MPa	2.5 MPa	5 MPa
Findley's power law	A	1.00E-14	1.54E-15	7.80E-17
	n	0.288	0.254	0.208
	$\varepsilon_0$	7.77E-4	1.09E-3	1.34E-3
	SS*	7.38E-7	1.50E-6	2.75E-6
	R <sup>2</sup>	0.538	0.910	0.580
Burgers	E <sub>M</sub> (MPa)	1.49E+6	6.74E+18	5.12E+20
	E <sub>K</sub> (MPa)	917.50	1565.20	2108.08
	$\eta_K$ (MPa.s)	880.60	1464.04	1877.59
	$\eta_M$ (MPa.s)	2.87E+6	5.58E+6	5.98E+6
	$\tau$ (s)	0.96	0.93	0.89
	SS*	1.50E-8	2.91E-8	3.11E-8
	R <sup>2</sup>	0.991	0.941	0.994

\* Sum of squares

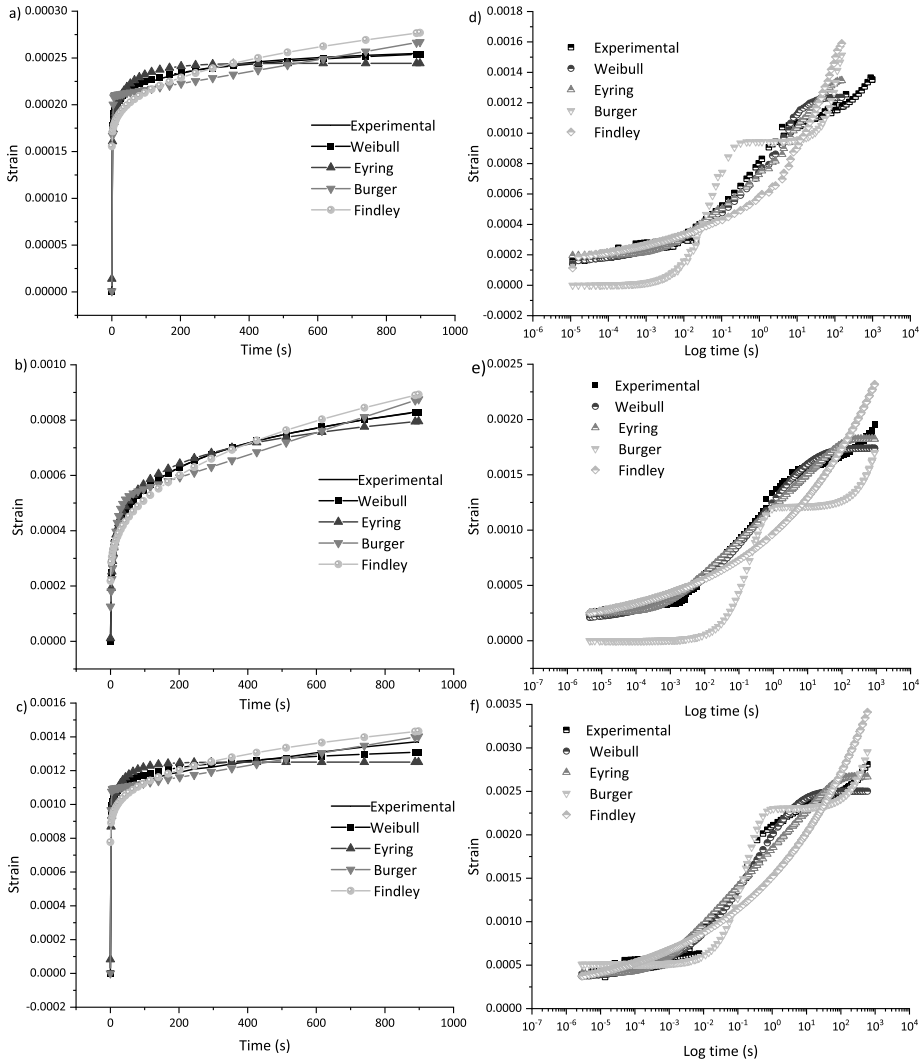


**Fig. 5** Viscoelastic fitting for the creep curves performed at **a)** 1 MPa, **b)** 2.5 MPa, **c)** 5 MPa; TTS curves using all analytical models for the following stress levels: **d)** 1 MPa, **e)** 2.5 MPa, and **f)** 5 MPa

The parameter  $\eta_M$  is the permanent viscous flow and probably the most important one since it represents the irrecoverable creep, i.e., it is a measure of the amount of residual strain left in the material after repeated creep and recovery. It is very sensitive to the temperature and applied stress. This parameter is associated with the viscous part of the material and to the damage of oriented noncrystalline regions (Yang et al. 2006b). This parameter decreases with increasing temperature and stress due to the greater mobility of the molecular chains at higher temperatures. A greater portion of molecules is necessary for molecular chain cooperativity when higher stress is applied; consequently, a higher deformation over time is obtained, which increases the permanent viscous flow (Lomellini 1992; Matsuoka 1993; Xu et al. 2010; Yang et al. 2006b; Fancey 2005; Lorandi et al. 2016).

The Weibull- and Eyring-based models (Eqs. (3) and (5), respectively; Fig. 5) are applied, and the results are presented in Table 2. The Weibull-based model suggests that latches are activated over time and the triggering time of each latch depends on the stiffness of the correspondent spring and viscosity of the dashpot (Fancey 2001, 2005). Under creep loading, triggering times are reduced as the creep load increases, thereby increasing the strain rate (in accordance with Fig. 2).

According to the Weibull model, the failure of the elements in a system allows relaxation of chain segments in amorphous materials, which is represented by time-dependent phenomena from the Weibull function. The parameter  $\varepsilon_C$  is referred to the cumulative number of activations with time, which increases with higher temperature and applied stress. Hence there is a progressive activation of latch elements since higher stress levels promote a higher number of these latches activated over time. In molecular terms, it can be associated with the number of chain segments that “work together” cooperatively to overcome any energetic barrier for molecular motion, that is, the viscoelastic changes occur through incremental jumps, in which segments of molecules jump between positions of relative stability; if there is no excitation (through higher stress or temperature), then the segments tend to remain deformed. This parameter is the characteristic lifetime where 63.2% of the elements have failed (calculated through time constant that characterizes the response of a linear time-invariant first-order system; see Fancey (2001)). This characteristic lifetime parameter is, physically speaking, the constant representing the required time for the system to respond to a decay to zero if the system keeps decaying at the initial rate due to progressive changes on the decay rate. This decay is mathematically represented by  $1/e$ . In the case of creep curves, as it is an increasing system, the response is given by  $1 - 1/e$ , that is, 63.2%.

The lower values obtained with the applied static stress level are due to a higher portion of the chain segments already activated due to a higher stress level imposed, which takes shorter times. The  $\beta_C$  is a shape parameter. The model consists of latches, the triggering time of each latch being dependent on the stiffness of the corresponding spring and viscosity of the dashpot. The values decrease with increasing stress and temperature. In mechanical terms (latch model), it means that higher strain rate allows a greater proportion of latches with longer triggering times to become activated during the creep cycle. In molecular terms, it is associated with broader (higher) relaxation times promoted by a higher number of segments that need to be activated together. Hence, the incremental step for the failure of the chain segments occurs for a more homogeneous manner, since the stretched exponential function is nearer to unity for low stress levels.

At the  $T_g$ , the values are nearer to one (within the 0–1 range) when compared to glassy and elastomeric states because the frozen-in segments store energy as heat and hence molecular motions occur in a fast and more cooperative manner. Aiming to better explain the  $T_g$  values, we utilized the Eyring-based model. At 210 °C the values are similar, given the fact that the chains are in high viscosity state (without energy storage). Considering that the stretched exponential is referred to the time relative to 63.2% of deformation, this deformation occurs in a narrower time for the same time interval when comparing the glassy and elastomeric regions (Fancey 2001, 2005; Almeida et al. 2018a, 2018b).

The parameters obtained for the TTS curves (Table 3 and Fig. 5) are discussed as follows:

- i. *Weibull*: the parameter  $\varepsilon_c$  keeps a similar magnitude order, and  $\varepsilon_i$  maintains higher values. The parameter  $\eta_c$  is below than those obtained using short-term tests. This is due to a higher number of chain segments already activated when the composite is in the viscous state. The parameter  $\beta_c$  is similar with the values obtained at the  $T_g$  for all stress levels;

**Table 2** Weibull and Eyring fitting at a) 50 °C, b) 150 °C, and c) 210 °C

Model tested at 50 °C		Parameters	1 MPa	2.5 MPa	5 MPa
Weibull	$\varepsilon_i$ (%)		1.51E-7	3.33E-7	1.77E-7
	$\varepsilon_c$ (%)		4.25E-4	6.49E-4	7.73E-4
	$\eta_c$		26680.49	37721.57	409.39
	$\beta_c$		0.085	0.064	0.057
	SS*		1.21E-10	7.99E-10	1.09E-9
	R <sup>2</sup>		0.998	0.993	0.995
Eyring	$\tau$ (s)		80.61	30.29	11.26
	$\sigma_e$ (MPa)		2.44E-4	3.36E-4	4.70E-4
	SS*		2.14E-9	7.01E-9	8.26E-9
	R <sup>2</sup>		0.965	0.939	0.962
Model tested at 150 °C		Parameters	1 MPa	2.5 MPa	5 MPa
Weibull	$\varepsilon_i$ (%)		-1.22E-6	-4.88E-6	-6.70E-6
	$\varepsilon_c$ (%)		2.22E-3	1.49E-3	1.99E-3
	$\eta_c$		26399.87	163.13	70.91
	$\beta_c$		0.2256	0.2813	0.2886
	SS*		6.31E-10	2.68E-9	7.64E-9
	R <sup>2</sup>		0.999	0.999	0.998
Eyring	$\tau$ (s)		34419.72	19097.23	11019.17
	$\sigma_e$ (MPa)		1.24E-3	1.72E-3	2.41E-3
	SS*		1.22E-8	2.51E-9	2.36E-9
	R <sup>2</sup>		0.989	0.999	0.999
Model tested at 210 °C		Parameters	1 MPa	2.5 MPa	5 MPa
Weibull	$\varepsilon_i$ (%)		2.69E-6	2.67E-6	1.61E-6
	$\varepsilon_c$ (%)		2.66E-3	3.58E-3	4.61E-3
	$\eta_c$		282022.52	98026.40	4451.65
	$\beta_c$		0.068	0.063	0.059
	SS*		2.37E-8	3.59E-8	4.02E-8
	R <sup>2</sup>		0.981	0.989	0.994
Eyring	$\tau$ (s)		52.70	31.63	15.04
	$\sigma_e$ (MPa)		1.25E-3	1.78E-3	2.57E-3
	SS*		1.31E-7	2.42E-7	3.08E-7
	R <sup>2</sup>		0.918	0.925	0.953

\* Sum of squares

- ii. *Eyring*: all parameters are coherent with those obtained using 10-min creep experiments, mainly when compared with glassy and rubbery states;
- iii. *Findley*: The constants  $A$  and  $n$  decrease in comparison to 10-min creep tests, whereas  $\varepsilon_0$  keeps similar values;

**Table 3** Viscoelastic parameters calculated for TTS curves performed at 1, 2.5, and 5 MPa

Models - TTS	Parameters	1 MPa	2.5 MPa	5 MPa
Weibull	$\varepsilon_i$ (%)	1.41E-4	1.68E-4	3.41E-4
	$\varepsilon_c$ (%)	1.09E-3	1.57E-3	2.16E-3
	$\eta_c$	1.81	0.58	0.35
	$\beta_c$	0.33	0.30	0.36
	SS*	1.21E-07	6.41E-07	1.18E-6
	R <sup>2</sup>	0.986	0.993	0.994
Eyring	$\tau$ (s)	292.54	55.42	39.82
	$\sigma_e$ (MPa)	1.35E-3	1.82E-3	2.67E-3
	SS*	6.06E-7	7.34E-7	2.07E-6
	R <sup>2</sup>	0.984	0.992	0.989
Findley	A	7.54E-21	4.96E-23	5.46E-22
	n	0.16	0.14	0.13
	$\varepsilon_0$	1.12E-4	9.07E-5	1.22E-4
	SS*	2.60E-6	6.73E-6	1.31E-5
	R <sup>2</sup>	0.932	0.927	0.931
Burger	$E_M$ (MPa)	-1.35E+42	-7.54E+8	9800.12
	$E_K$ (MPa)	5304.77	4128.55	2789.18
	$\eta_K$ (MPa.s)	294.45	923.43	502.99
	$\eta_M$ (MPa.s)	8.57E+6	9.13E+6	4.59E+6
	SS*	9.27E-6	2.98E-5	3.35E-6
	R <sup>2</sup>	0.758	0.677	0.983

\* Sum of squares

iv. *Burger*:  $\eta_M$  and  $E_K$  keep similar values to those obtained with 10-min creep tests. The parameter  $E_M$  is higher, and  $\eta_K$  is lower than those obtained using short-term experiments. Both parameters are temperature- and stress-dependent, and thus are expected to have different values.

## 5 Conclusions

In this study, a complete structure *versus* property relationship of a high-performance non-crimp carbon fiber composite laminate is presented. Four different models are employed to predict the creep response in the glassy, glass transition, and rubbery states: the Findley, Burger, Weibull, and Eyring models. Three different stress levels and ten different temperatures were analyzed. The results demonstrate that short-term creep experiments (10-min) have similar values to 2-day creep experiments. The Weibull and Eyring models show better fittings to the experimental data than those of Burger and Findley. For all models, better predictions are found at the  $T_g$  region for all applied stresses. The prediction using time-temperature superposition curves are also successfully applied, but the Findley and Burger models do not fit well the data. Nevertheless, the Weibull and Eyring models fit very well the experimental data, except for region III. At last, the data presented here allow a better knowledge of the microstructural creep behavior of laminated composites over the time and their response under several temperature and stress conditions.

**Acknowledgements** The authors are grateful to CNPq (process number 153335/2018-1), FAPESP (process number 2006/02121-6), and CAPES for the financial support.

**Funding Note** Open access funding provided by Aalto University.

**Publisher's Note** Springer Nature remains neutral with regard to jurisdictional claims in published maps and institutional affiliations.

**Open Access** This article is licensed under a Creative Commons Attribution 4.0 International License, which permits use, sharing, adaptation, distribution and reproduction in any medium or format, as long as you give appropriate credit to the original author(s) and the source, provide a link to the Creative Commons licence, and indicate if changes were made. The images or other third party material in this article are included in the article's Creative Commons licence, unless indicated otherwise in a credit line to the material. If material is not included in the article's Creative Commons licence and your intended use is not permitted by statutory regulation or exceeds the permitted use, you will need to obtain permission directly from the copyright holder. To view a copy of this licence, visit <http://creativecommons.org/licenses/by/4.0/>.

## References

- Alderliesten, R.C.: How proper similitude can improve our understanding of crack closure and plasticity in fatigue. *Int. J. Fatigue* (2015). <https://doi.org/10.1016/j.ijfatigue.2015.04.011>
- Almeida Jr, J.H.S., Ornaghi Jr, H.L., Lorandi, N., Bregolin, B.P., Amico, S.C.: Creep and interfacial behavior of carbon fiber reinforced epoxy filament wound laminates. *Polym. Compos.* **39**(S4), E2199–E2206 (2018a). <https://doi.org/10.1002/pc.24537>
- Almeida Jr, J.H.S., Ornaghi Jr, H.L., Lorandi, N., Marinucci, G., Amico, S.C.: On creep, recovery, and stress relaxation of carbon fiber-reinforced epoxy filament wound composites. *Polym. Eng. Sci.* **58**(19), 1837–1842 (2018b). <https://doi.org/10.1002/pen.24790>
- Alrahlah, A., Khan, R., Alotaibi, K., Almutawa, Z., Fouad, H., Elsharawy, M., Silikas, N.: Simultaneous evaluation of creep deformation and recovery of bulk-fill dental composites immersed in food-simulating liquids. *Materials* **11**(7), 1–12 (2018). <https://doi.org/10.3390/ma11071180>
- Fancey, K.S.: A latch-based Weibull model for polymeric creep and recovery. *J. Polym. Eng.* **21**(6), 489–510 (2001). <https://doi.org/10.1515/POLYENG.2001.21.6.489>
- Fancey, K.S.: A mechanical model for creep, recovery and stress relaxation in polymeric materials. *J. Mater. Sci.* **2**, 2–6 (2005). <https://doi.org/10.1007/s10853-005-2020-x>
- Findley, W.N., Davis, F.A.: Creep and relaxation of nonlinear viscoelastic materials. In: Courier Corporation, vol. 1 (2013). [https://doi.org/10.1016/0032-3861\(78\)90187-8](https://doi.org/10.1016/0032-3861(78)90187-8)
- Gao, J., Sha, A., Wang, Z., Hu, L., Yun, D., Liu, Z., Huang, Y.: Characterization of carbon fiber distribution in cement-based composites by Computed Tomography. *Constr. Build. Mater.* **177**, 134–147 (2018). <https://doi.org/10.1016/j.conbuildmat.2018.05.114>
- Gates, T.S., Veazie, D.R., Brinson, L.C.: Creep and physical aging in a polymeric composite: comparison of tension and compression. *J. Compos. Mater.* (1997). <https://doi.org/10.1177/002199839703102404>
- Guedes, R.M.: Lifetime predictions of polymer matrix composites under constant or monotonic load. *Composites, Part A, Appl. Sci. Manuf.* **37**, 703–715 (2006). <https://doi.org/10.1016/j.compositesa.2005.07.007>
- Hu, H., Sun, C.T.: The characterization of physical aging in polymeric composites. *Compos. Sci. Technol.* **60**(14), 2693–2698 (2000). [https://doi.org/10.1016/S0266-3538\(00\)00127-5](https://doi.org/10.1016/S0266-3538(00)00127-5)
- Khan, R., Alderliesten, R., Badshah, S., Benedictus, R.: Effect of stress ratio or mean stress on fatigue delamination growth in composites: critical review. *Compos. Struct.* **124**, 214–227 (2015). <https://doi.org/10.1016/j.compstruct.2015.01.016>
- Lomellini, P.: Williams—Landel—Ferry versus Arrhenius behaviour: polystyrene melt viscoelasticity revised. *Polymer* **33**(23), 4983–4989 (1992)
- Lorandi, N.P., Cioffi, M.O.H., Ornaghi, H.L.: Dynamic Mechanical Analysis (DMA) of polymeric composite materials (Análise Dinâmica-Mecânica de Materiais Compósitos Poliméricos). *Sci. Ind.* **4**(48), 48–60 (2016)
- Lorandi, N.P., Cioffi, M.O.H., Shigue, C., Ornaghi, H.L.: On the creep behavior of carbon/epoxy non-crimp fabric composites. *Mater. Res.* **21**(3), e20170768 (2018). <https://doi.org/10.1590/1980-5373-MR-2017-0768>

- Mano, J.F., Sencadas, V., Costa, A.M., Lanceros-Méndez, S.: Dynamic mechanical analysis and creep behaviour of  $\beta$ -PVDF films. *Mater. Sci. Eng. A* **370**(1), 336–340 (2004). <https://doi.org/10.1016/j.msea.2002.12.002>
- Matsuoka, S.: Relaxation phenomena in polymers. *Polym. Int.* **32**(3), 435–438 (1993). <https://doi.org/10.1177/107769909307000320>
- Mohammad, S., Zamani, M., Behdinin, K.: Multiscale modeling of the mechanical properties of Nextel 720 composite fibers. *Compos. Struct.* **204**(July), 578–586 (2018). <https://doi.org/10.1016/j.compstruct.2018.08.001>
- Monticeli, F.M., Almeida, J.H.S. Jr., Neves, R.M., Ornaghi, F.G., Ornaghi, H.L. Jr.: On the 3D void formation of hybrid carbon/glass fiber composite laminates: a statistical approach. *Composites, Part A, Appl. Sci. Manuf.* **137**, 106036 (2020). <https://doi.org/10.1016/j.compositesa.2020.106036>
- Ornaghi Jr, H.L., Zattera, A.J., Amico, S.C.A.: Dynamic mechanical properties and correlation with dynamic fragility of sisal reinforced composites. *Polym. Compos.* **36**(1), 161–166 (2015). <https://doi.org/10.1002/pc.22925>
- Ornaghi Jr, H.L., Neves, R.M., Monticeli, F.M., Almeida Jr, J.H.S.: Viscoelastic characteristics of carbon fiber-reinforced epoxy filament wound laminates. *Compos. Commun.* **21**, 100418 (2020). <https://doi.org/10.1016/j.coco.2020.100418>
- Struik, L.C.: Physical aging in plastics and other glassy materials. *Polym. Eng. Sci.* **17**(3), 165–173 (1977)
- Sullivan, J.L.: Creep and physical aging of composites. *Compos. Sci. Technol.* **39**(3), 207–232 (1990). [https://doi.org/10.1016/0266-3538\(90\)90042-4](https://doi.org/10.1016/0266-3538(90)90042-4)
- Sullivan, J.L., Blais, E.J., Houston, D.: Physical aging in the creep behavior of thermosetting and thermoplastic composites. *Compos. Sci. Technol.* **47**, 389–403 (1993)
- Wang, B., Zhang, K., Zhou, C., Ren, M., Gu, Y., Li, T.: Engineering the mechanical properties of CNT/PEEK nanocomposites. *RSC Adv.* **9**, 12836–12845 (2019). <https://doi.org/10.1039/c9ra01212e>
- Xu, Y., Wu, Q., Lei, Y., Yao, F.: Creep behavior of bagasse fiber reinforced polymer composites. *Bioresour. Technol.* **101**(9), 3280–3286 (2010). <https://doi.org/10.1016/j.biortech.2009.12.072>
- Yang, J.L., Zhang, Z., Schlarb, A.K., Friedrich, K.: On the characterization of tensile creep resistance of polyamide 66 nanocomposites. Part I. Experimental results and general discussions. *Polymer* **47**(8), 2791–2801 (2006a). <https://doi.org/10.1016/j.polymer.2006.02.065>
- Yang, J.L., Zhang, Z., Schlarb, A.K., Friedrich, K.: On the characterization of tensile creep resistance of polyamide 66 nanocomposites. Part II: Modeling and prediction of long-term performance. *Polymer* **47**(19), 6745–6758 (2006b). <https://doi.org/10.1016/j.polymer.2006.07.060>